5th International Conference on Multiphase Flow, ICMF'04
Yokohama, Japan, May 30–June 4, 2004
Paper No. 457

# Discrete Particle Simulation of a Spout-Fluid Bed: Treatment of two-way Coupling and Effect of Drag Closure

**Jeroen M. Link[1], Niels G. Deen[1] and J.(Hans)A.M. Kuipers[1]**

1: Faculty of Science and Technology, University of Twente, Enschede, The Netherlands, J.M.Link@utwente.nl

**Abstract** A new method is proposed to map properties between the Lagrangian and Eulerian grid in a discrete particle model. The model was used to study the gas-particle flow in a spout-fluid bed and assess grid independency of the computations. Comparison between experimental and numerical results using various drag models revealed that the most frequently used drag model (i.e. the Ergun equation for low porosities and the Wen and Yu relation for high porosities) is less suitable for modeling fluid beds with stable high velocity jets, as encountered in spout(-fluid) beds. The Koch and Hill (2001) relation and the minimum of the relations of Ergun, and Wen and Yu are more suitable, although the former is preferred because of its more fundamental basis.

## 1. Introduction

Spout-fluid beds are used for a variety of processes involving particulate solids, like coating, drying, granulation and pyrolysis. The spout-fluid bed combines a number of favorable properties of both spouted and fluidized beds. Unfortunately a detailed understanding of the fundamentals of spout-fluid beds is lacking.

In early numerical studies (f.i. Littman *et al.*, 1985) only the overall behavior of the bed was considered neglecting the details of particle motion. Only recently Kawaguchi *et al.* (2000) and Link *et al.* (2004) used a discrete particle model to carry out a detailed study of the particle behavior in respectively a spouted bed and a spout-fluid bed. They solved the volume-averaged Navier-Stokes equations for the gas phase, taking momentum transfer between the gas and the particles into account. Newton's second law was used to compute the motion of each individual particle.

In this work, the discrete particle model originally developed by Hoomans *et al.* (1996) is used to study the particle dynamics in a spout-fluid bed. The spout-fluid bed poses some challenges for the discrete particle model: a steep velocity gradient in the gas phase is present near the spout region and the particle Reynolds numbers, especially near the spout mouth, are much higher than those in regular (bubbling) fluidized beds.

In this paper a new method is introduced to calculate the porosity and the forces acting on a particle in a grid-independent manner. This method is used to assess grid-independency of the computed gas phase flow field. In addition several drag relations are tested for their suitability to describe the drag force in spout-fluid beds by comparing the numerical results with experimentally determined pressure drop fluctuations and particle flux profiles.

**Table 1** Particle properties.

| | | |
|---|---|---|
| $\rho_p$ | 2526 | kg/m$^3$ |
| $u_{mf}$ | 1.28 | m/s |
| $e_{n,\,p\leftrightarrow p}$ | 0.97 | - |
| $e_{n,\,p\leftrightarrow w}$ | 0.97 | - |
| $\mu_{p\leftrightarrow p}$ | 0.10 | - |
| $\mu_{p\leftrightarrow w}$ | 0.10 | - |
| $\beta_{0,\,p\leftrightarrow p}$ | 0.33 | - |
| $\beta_{0,\,p\leftrightarrow w}$ | 0.33 | - |

## 2. Theory of the Model

The discrete particle model (DPM) used in this work is based on the hard-sphere model developed by Hoomans *et al.* (1996). A short description of the model is given in this section. For further

details the interested reader is referred to Hoomans *et al.* (1996).

In the DPM rigid particles are assumed to interact through binary, instantaneous collisions. Particle collision dynamics are described by collision laws, which account for energy dissipation due to non-ideal particle interaction by means of the empirical coefficients of normal and tangential restitution and the coefficient of friction. The particle collision characteristics play an important role in the overall bed behaviour as was shown by Goldschmidt *et al.* (2001). For this reason the collision parameters, for both particle-particle and particle-wall collisions, were accurately determined by separate impact experiments and subsequently used in our simulations. An overview of the particle properties including the collision parameters is given in Table 1.

The motion of each individual particle present in the system is calculated from the Newtonian equation of motion:

$$m_p \frac{d\mathbf{v}_p}{dt} = -V_p \nabla p + \frac{V_p \beta}{\varepsilon_p}(\mathbf{u}_f - \mathbf{v}_p) + m_p \mathbf{g} \tag{1}$$

where $\beta$ represents the inter-phase momentum transfer coefficient due to drag. Several drag relations to calculate $\beta$ are available and will be discussed later.

The gas phase flow field is computed from the volume-averaged Navier-Stokes equations:

$$\frac{\partial}{\partial t}(\varepsilon_f \rho_f) + \nabla \cdot (\varepsilon_f \rho_f \mathbf{u}_f) = 0 \tag{2}$$

$$\frac{\partial}{\partial t}(\varepsilon_f \rho_f \mathbf{u}_f) + \nabla \cdot (\varepsilon_f \rho_f \mathbf{u}_f \mathbf{u}_f) = -\varepsilon_f \nabla p - \nabla \cdot (\varepsilon_f \boldsymbol{\tau}_f) - \mathbf{S}_p + \varepsilon_f \rho_f \mathbf{g} \tag{3}$$

where the viscous stress tensor, $\boldsymbol{\tau}_f$ is assumed to obey the general form for a Newtonian fluid (Bird *et al.*, 1960):

$$\boldsymbol{\tau}_f = -\left[\left(\lambda_f - \frac{2}{3}\mu_f\right)(\nabla \mathbf{u}_f)\mathbf{I} + \mu_f\left((\nabla \mathbf{u}_f) + (\nabla \mathbf{u}_f)^T\right)\right] \tag{4}$$

Two-way coupling is achieved via the sink term, $\mathbf{S}_p$, which is computed from:

$$\mathbf{S}_p = \frac{1}{V_{cell}} \sum_{\forall i \in cell} \frac{V_i \beta}{\varepsilon_p}(\mathbf{u}_f - \mathbf{v}_i) D(\mathbf{r} - \mathbf{r}_i) \tag{5}$$

with $\varepsilon_p = 1 - \varepsilon_f$. The distribution function, $D$ distributes the reaction force acting on the gas phase to the velocity nodes in the (staggered) Eulerian grid.

### 2.1 Momentum exchange coefficient

The calculation of the momentum exchange coefficient, $\beta$ is vital for an adequate description of (spout-)fluid beds and can be performed using several drag models. The most frequently used drag model in discrete particle models (Kawaguchi *et al.*, 2000 and Hoomans *et al.*, 1996) is a combination of the Ergun equation, originally developed for packed beds, at low porosities ($\varepsilon_f < 0.8$):

$$\beta_{Ergun} = 150\frac{\varepsilon_p^2}{\varepsilon_f}\frac{\mu_f}{d_p^2} + 1.75\varepsilon_p\frac{\rho_f}{d_p}\left|\mathbf{u}_f - \mathbf{v}_p\right| \tag{6}$$

and the Wen and Yu relation at high porosities ($\varepsilon_f > 0.8$):

$$\beta_{Wen\&Yu} = \frac{3}{4}C_D\varepsilon_p\frac{\rho_f}{d_p}\left|\mathbf{u}_f - \mathbf{v}_p\right|\varepsilon_f^{-1.65} \tag{7}$$

where $C_D$ is the drag coefficient given by Schiller and Naumann (1933):

$$\begin{cases} C_D = \dfrac{24}{\mathrm{Re}_p}(1 + 0.15\,\mathrm{Re}_p^{0.687}) & \mathrm{Re}_p < 1000 \\ C_D = 0.44 & \mathrm{Re}_p > 1000 \end{cases} \tag{8}$$

Recently Koch and Hill (2001) proposed a new drag relation based on lattice-Boltzmann simulations:

$$\beta_{Koch\&Hill} = \frac{18\mu_f\varepsilon_f^2\varepsilon_p}{d_p^2}\left(F_0(\varepsilon_p) + \tfrac{1}{2}F_3(\varepsilon_p)\,\mathrm{Re}_p\right) \tag{9}$$

with

$$\mathrm{Re}_p = \frac{\varepsilon_f\rho_f\left|\mathbf{u}_f - \mathbf{v}_p\right|d_p}{\mu_f} \tag{10}$$

$$\begin{cases} F_0(\varepsilon_p) = \dfrac{1 + 3\sqrt{\dfrac{\varepsilon_p}{2}} + \dfrac{135}{64}\varepsilon_p\ln(\varepsilon_p) + 16.14\varepsilon_p}{1 + 0.681\varepsilon_p - 8.48\varepsilon_p^2 + 8.16\varepsilon_p^3} & \varepsilon_p < 0.4 \\ F_0(\varepsilon_p) = \dfrac{10\varepsilon_p}{\varepsilon_f^3} & \varepsilon_p > 0.4 \end{cases} \tag{11}$$

$$F_3(\varepsilon_p) = 0.0673 + 0.212\varepsilon_p + \frac{0.0232}{\varepsilon_f^5} \tag{12}$$

## 3. Numerical implementation

The equations for the gas phase are coupled with those of the particle phase through the porosity and the interphase momentum exchange. All relevant quantities should be averaged over a volume, which is large compared to the size of the particles, and in such way that they are independent of the Eulerian grid size.

### 3.1 Calculation of the porosity

A straightforward method for the calculation of the porosity was given by Hoomans *et al.* (1996). In their work, the porosity in an Eulerian cell is calculated as follows:

$$\varepsilon_{f,cell} = 1 - \frac{1}{V_{cell}} \sum_{\forall i \in cell} f_{cell}^{i} V_{p}^{i} \tag{13}$$

where $f_{cell}^{i}$ is the volume fraction of particle *i* in the cell under consideration. This method works well when the size of the grid cells is much larger than that of the particles (i.e. $V_{cell} >> V_p$). From a numerical point of view however it is sometimes desirable to use small computational cells in order to resolve all relevant details of the gas flow and to obtain a grid-independent solution. Unfortunately, the method of Hoomans *et al.* (1996) generates problems once $V_{cell}$ approaches $V_p$. That is, grid cells can be fully occupied by a particle, which leads to numerical problems. In order to overcome this problem, we suggest a new method to calculate the porosity.

In order to prevent numerical problems, the particles are represented as porous cubes with a size taken as the ratio of the cube diameter and the particle diameter:

$$a = \frac{d_{cube}}{d_p} \tag{14}$$

The porosity of the cube can easily be calculated as:

$$\varepsilon_{cube} = \frac{V_p}{V_{cube}} = \frac{\pi}{6a^3} \tag{15}$$

Finally the method of Hoomans *et al.* (1996) to calculate the gas fraction in a cell is adapted to facilitate the porous cube representation:

$$\varepsilon_{f,cell} = 1 - \varepsilon_{cube} \sum_{\forall i \in cell} f_{cell}^{i} \tag{16}$$

where $f_{cell}^{i}$ is the volume fraction of the cell under consideration that is occupied by cube *i*. By representing the particle as a porous cube, its presence is felt only weakly in a relatively large portion of the flow domain. Consequently, grid refinement will not lead to local extremes in the gas-fraction around the center of mass of the particle.

The advantage of the new porosity mapping method is illustrated in Fig. 1. This figure shows that the results of the new method are consistent, although minor scattering near the walls can be observed, whereas the method used by Hoomans *et al.* (1996) exhibits scattering over the entire width of the bed when the grid is refined. Both methods produce similar results for coarse grids.

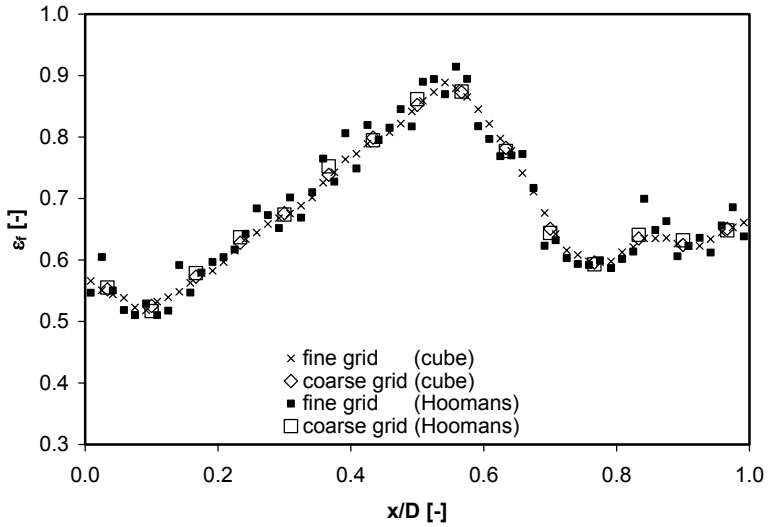


**Fig. 1.** Porosity profile of a particle configuration determined with the new method and the method used by Hoomans *et al.* (1996) for a fine grid ($d_{cell}/d_p = 1.0$) and a coarse grid ($d_{cell}/d_p = 4.0$).

### 3.2 Coupling of the forces between the phases

The force balance for a single particle, which is used in our model to calculate the acceleration of the particle is given by Eq. (1). Most of the variables in this equation are only available on the Eulerian grid. The acceleration of the particle should however be available on the Lagrangian grid. In order to calculate the acceleration of the particle, these variables need to be mapped to the position of the particle. In order to satisfy Newton's third law, a consistent mapping technique should be used for the calculation of the momentum exchange coefficient, $\beta$. Hoomans *et al.* (1996) used a volume weighing technique for the mapping. Unfortunately, this technique can generate problems: when the grid is refined, the volume of the gas phase to which the force is distributed becomes smaller, which leads to numerical problems.

For a proper treatment of the drag force, the control volume used in the calculations should match the control volume for which the drag relation was derived. Generally the control volume will be much larger than the particle size (i.e. $a$ = 3-5). For the calculation of the acceleration of the particle we suggest a method similar to that of the porosity mapping.

A general variable $\phi_{cell}$ on the Eulerian grid can be mapped to a property $\phi_p$ on the Lagrangian position of the particle using the following equation:

$$\phi_p = \frac{1}{V_{cube}} \sum_{\forall j \in cube} f_j^{cube} V_j \phi_j \tag{17}$$

where $f_j^{cube}$ is the volume fraction of cell $j$ occupied by the cube.

On the other hand, a general variable $\phi_i$ at a Lagrangian position can be mapped to an Eulerian property $\phi_{cell}$ using the following equation:

$$\phi_{cell} = V_{cell} \sum_{\forall i \in cell} \frac{f_{cell}^i \phi_i}{V_i} \tag{18}$$

where $f_{cell}^i$ is the volume fraction of the cell under consideration that is occupied by cube $i$.

# 4. Results

## 4.1 Test cases

The model that was described in the preceding sections was applied to simulate the flow in a pseudo 2D spout-fluid bed. The simulation results were compared with dynamic pressure drop measurements and digital images capturing the bed structure. In order to enable a quantitative comparison, a frequency spectrum was obtained by applying fast Fourier transformation to the dynamic pressure drop signals.

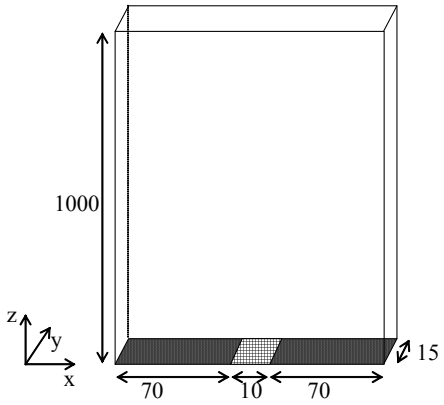


**Fig. 2.** Schematic representation of the pseudo-2D set-up (dimensions in mm).

A schematic representation of the pseudo-2D gas-fluidized bed used in this study, along with its dimensions, is given in Fig. 2. The bed is 6 particle diameters (15 mm) deep to prevent bridge formation (stable particle configurations extending from wall to wall). The depth of the bed is assumed to be sufficiently small to display pseudo-2D behavior, which is necessary to enable the use of digital image analysis as a whole field measuring technique.

The front wall of the bed consists of a glass plate to permit visual observation of the particle motion inside the bed. The side walls of the bed are made of aluminum strips and the back wall is made of polycarbonate.

Pressurized air is fed to the bed through three separate sections. A 3 mm thick porous plate with an average pore size of 10 microns provides a homogeneous gas distribution over the two porous sections. A 0.5 mm metal gauze covers the spout mouth located in between the two porous sections. The gas flow rate in each section was controlled by mass flow controllers and rapidly responding magnetic valves.

A high frequency pressure probe (Kulite XT-190M-0.35BAR VG) was used to measure the pressure drop over the bed contents at a frequency of 100 Hz. The probe was positioned in the middle of the back wall of the bed about 1 cm above the porous plate.

Digital images were recorded with a 262 Hz CCD camera (Dalsa CA-D6) equipped with a 12.5 mm lens. The aperture of the camera was set to f4 and the exposure time was fixed at 3.8 ms. The recorded images consist of 532 x 516 8-bit pixels. The image quality depends on the illumination conditions of the bed, which should be strong and continuous. This was accomplished with the use of two 500 W halogen lamps positioned along each side of the camera, which were illuminating the bed under a small angle (< 45º), preventing undesirable reflections. The digital images were analyzed to measure both the particle velocity and the particle volume fraction, from which the particle flux could be calculated. A detailed description of this technique can be found Link *et al.* (2004).

Two test cases corresponding to different regimes were investigated. In both cases the pseudo-2D set-up was filled with $2.45.10^3$ particles with a diameter of 2.5 mm. The properties of the particles that were used are given in Table 1. In the simulations the height of the column was reduced to 75 cm. In case 1, the bubbling spout regime was investigated ($u_{bg}$ = 1.5 m/s and $u_{sp}$ = 30.0 m/s). Case 2 comprised the meandering spout regime ($u_{bg}$ = 3.0 m/s and $u_{sp}$ = 20.0 m/s).

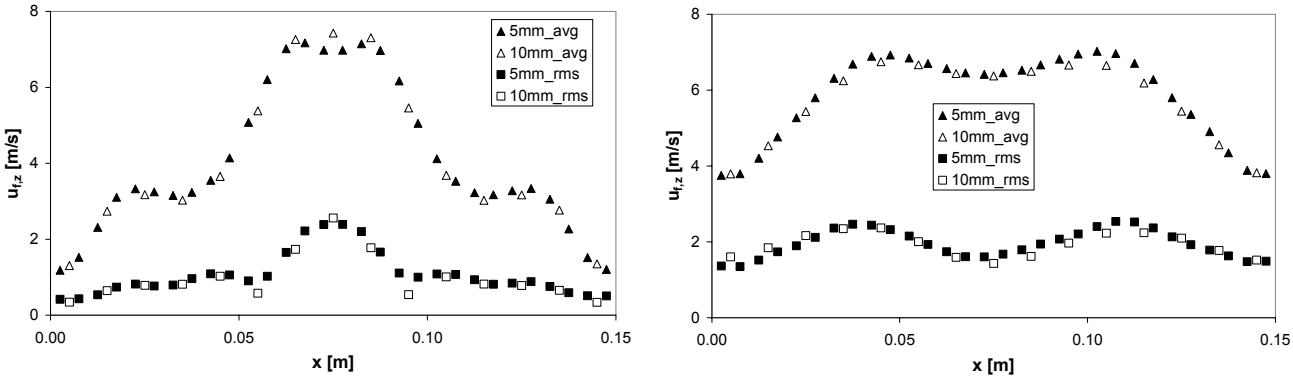


Case 1, bubbling spout Case 2, meandering spout

**Fig. 3.** Profiles of the time-averaged vertical gas velocity and associated fluctuations at a height of 0.15 m for two sizes of the computational grid.

### 4.2 Grid resolution

In a spout-fluid bed large gas velocity gradients are present near the spout necessitating the use of a sufficiently refined grid.

In order to check whether the computational grid is fine enough to produce accurate results, its influence was studied using the test cases described above. Both test cases were simulated using identical start-up conditions except for the size of the computational grid, which was set to 5 mm and 10 mm for both cases.

A period of 20 s was simulated using the Koch and Hill (2001) drag relation. During the last 16 s the average vertical gas velocity (Fig. 3), the average particle flux (Fig. 4) and pressure drop fluctuations (Fig. 5) with associated frequency spectra (Fig. 6) were calculated.

Fig. 3 shows that for both cases the average gas velocity and its fluctuations are hardly influenced by the choice of the computational grid. As can be expected, the resulting particle fluxes in Fig. 4 display even less sensitivity with respect of the computational grid. The pressure drop fluctuations in Fig. 5 show small differences between the two grids. Also the frequency spectra shown in Fig. 6 show minor differences in the obtained dominant frequencies. Since the size of the computational cells hardly influences the results, but significantly influences computation time, a grid size of 10 mm has proven to be sufficiently accurate for further numerical study.

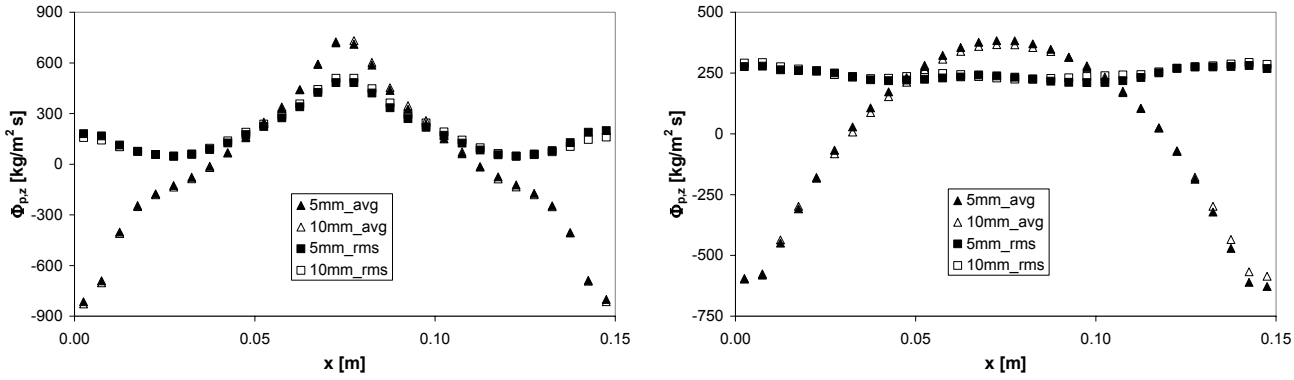


Case 1, bubbling spout Case 2, meandering spout

**Fig. 4.** Profiles of the time-averaged vertical particle flux and associated fluctuations at a height of 0.15 m for two computational grids.

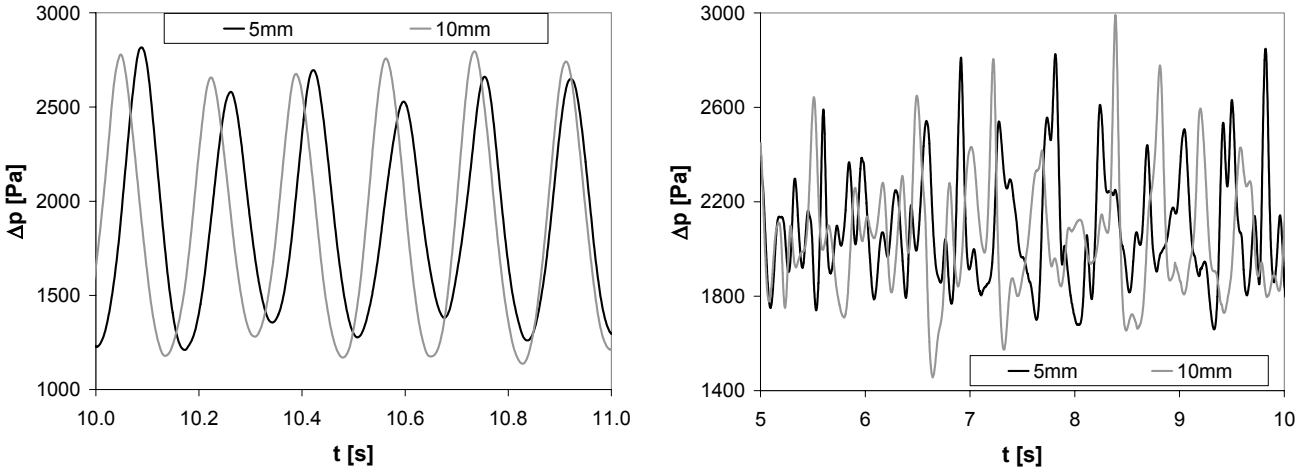


Case 1, bubbling spout Case 2, meandering spout

**Fig. 5.** Simulated pressure drop signal for two computational grids.

### 4.3 Drag relation

All drag relations depend highly on the particle Reynolds number, $Re_p$. In order to select a proper drag relation, information on the range of $Re_p$, in which a (spout-)fluid bed is operated, is required. Fig. 7 shows the range of $Re_p$ that was determined by monitoring its distribution over a period of 1 s during a DPM simulation. Both test cases were studied and the Koch and Hill (2001) drag relation was used. It can be seen that most particles (97%) have a relatively high Reynolds-number, i.e. between 200 and 10,000.

In this range of $Re_p$ the dimensionless drag forces resulting from Eqs. (6-12) were calculated (Fig. 8). At these $Re_p$ the Ergun (1952), and Wen and Yu (1966) relations predict differences in drag forces up to a factor of four. Therefore combining these relations at $\varepsilon_f = 0.8$ will result in a large discontinuity in the drag force at high $Re_p$, which has no physical background and may cause numerical instabilities.

The Koch and Hill relation predicts values in between the Ergun and Wen and Yu relations and can therefore be considered as an alternative. Another way to overcome the discontinuity is to use the minimum of the Ergun and Wen and Yu relations.

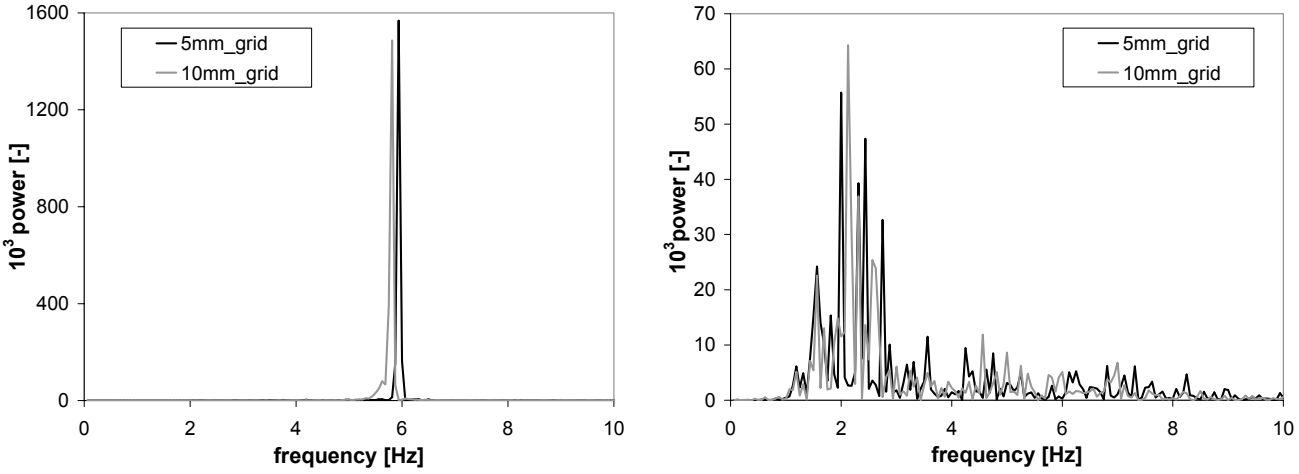


Case 1, bubbling spout Case 2, meandering spout

**Fig. 6.** Simulated frequency spectra of pressure drop fluctuations for two computational grids.

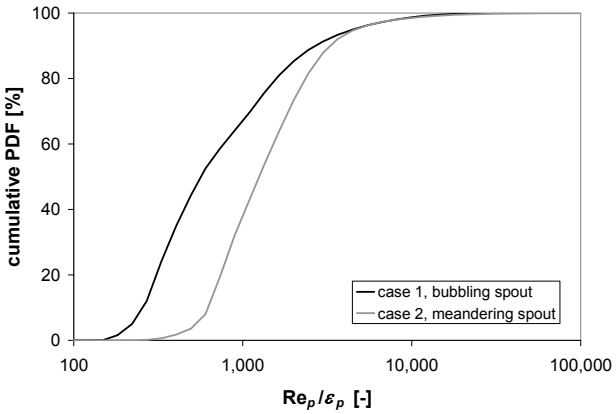


**Fig. 7.** Typical particle Reynolds numbers for a spout-fluid bed.

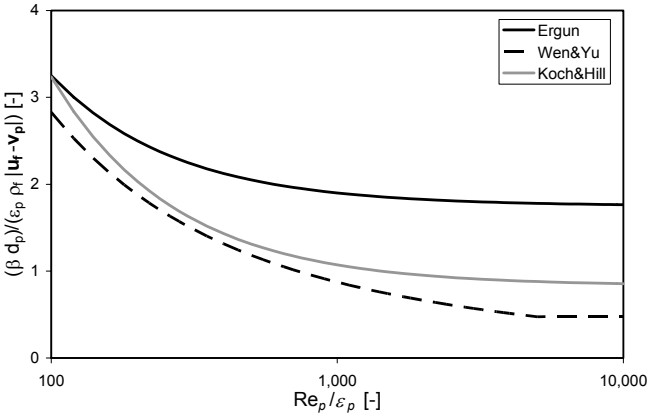


**Fig. 8.** Dimensionless drag for several drag relations at $\varepsilon_f = 0.8$.

To determine which drag relation is most suitable to model a spout-fluid bed, simulations were carried out for both test cases using the following drag models:

- Case old; if $\varepsilon_f < 0.8$ the Ergun equation is used, otherwise the Wen and Yu relation is used.
- Case Koch&Hill; the relation of Koch and Hill (2001) given in Eq. (9) is used.
- Case minimum; the minimum of the Ergun, and Wen and Yu equations is used.

In all simulations a value of 5 was used for the ratio between the cube size and the particle diameter, $a$. The computed and experimentally obtained pressure drop fluctuations and the associated frequency spectra are respectively shown in Fig. 9 and 10. The former shows a periodically fluctuating pressure drop for the Koch and Hill model, the minimum model and the experiments, while the old model displays a more irregular pattern. These results are also reflected in the power spectra. That is to say that except for the old model a dominant frequency around 5 to 6 Hz is found. In the case of the meandering spout, the differences between the drag models are less pronounced. Each of the models predicts a randomly meandering spout, which leads to an irregular pressure drop signal. Only the old model predicts a dominant peak around 2.5 Hz.

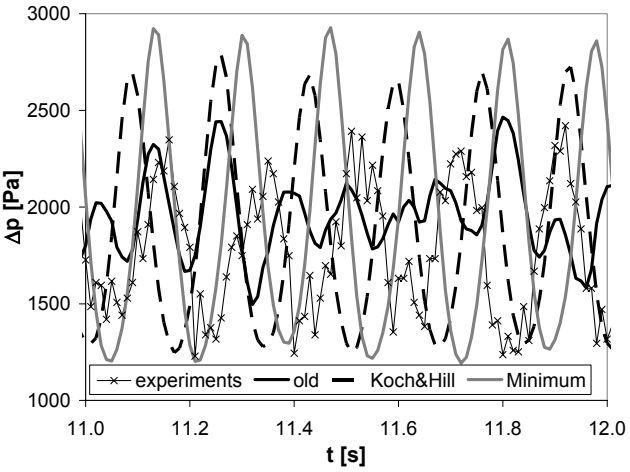


Case 1, bubbling spout

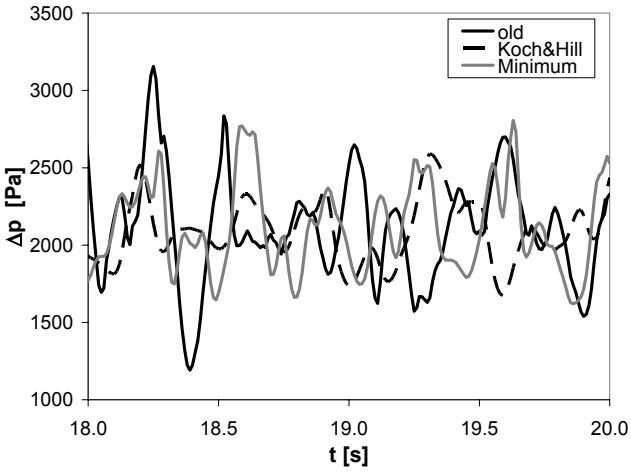


Case 2, meandering spout

**Fig. 9.** Experimental and computed pressure drop fluctuations.

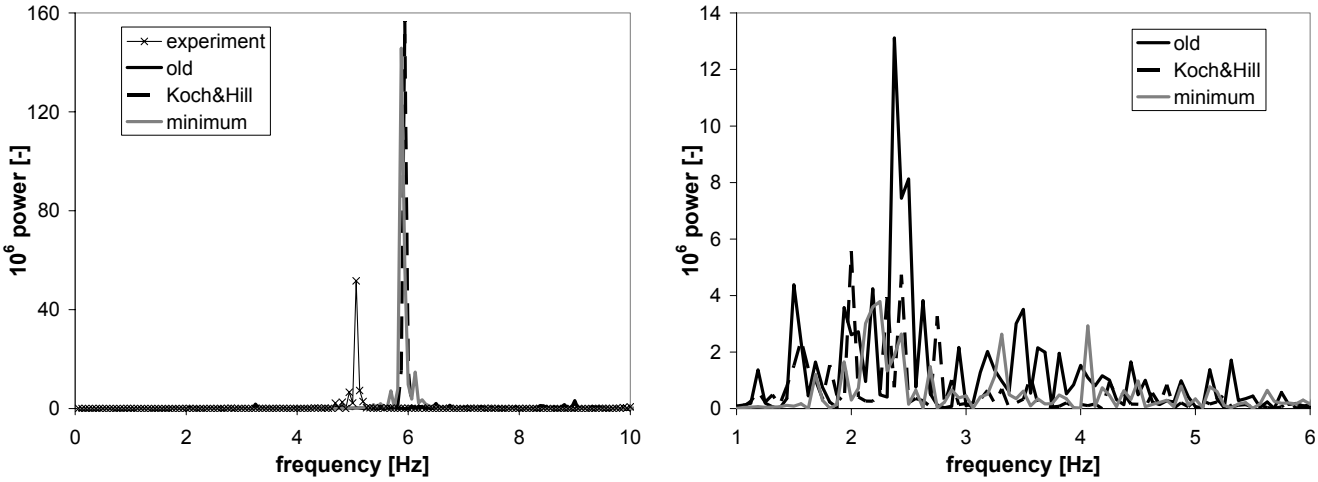


Case 1, bubbling spout Case 2, meandering spout

**Fig. 10.** Experimental and computed frequency spectra of pressure drop fluctuations.

Particle flux profiles that were measured for both cases are shown in Fig. 11, along with the corresponding computational results. For case 1 a narrow peak is found in the particle flux profile, which is well captured by both the Koch and Hill model and the minimum model. However, the old model shows a much broader peak. The deviating results obtained from the old model can be explained by considering Fig. 8. The old model predicts very large drag forces in the annulus, where $\varepsilon_f < 0.8$, and low drag forces in the spout, where $\varepsilon_f > 0.8$. The old model predicts the behavior of a system, which is associated with a higher background velocity and a lower spout velocity, like case 2. For case 2, very similar particle flux profiles are found for all models. The agreement with the experimental result is quite good.

## 5. Conclusions

In this work, a new method was introduced to overcome problems in the coupling between the phases in an Euler-Lagrange model. With the new method, the computational grid can be refined to the scale of the particles, without causing extrema in the porosity and the associated drag force. The new method was successfully incorporated in the Euler-Lagrange model and used to simulate two different flow regimes in a spout-fluid bed. It was found that contrary to the method of Hoomans *et al.* (1996), grid independent results could be obtained.

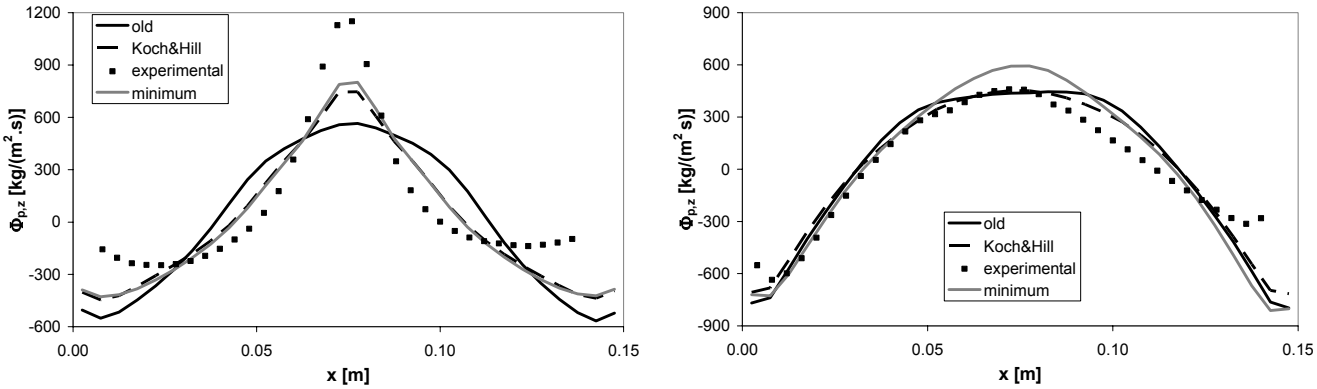


Case 1, bubbling spout Case 2, meandering spout

**Fig. 11.** Experimental and computed particle flux profiles at a height of 0.10 m.

Numerical results using various drag models were compared with experimental pressure signals. It was found that the most frequently used drag model (i.e. the Ergun equation for low porosities and the Wen and Yu relation for high porosities) is less suitable for modeling fluid beds with stable high velocity jets, as encountered in spout(-fluid) beds. The minimum of the relations of Ergun, and Wen and Yu, as well as the relation proposed by Koch and Hill (2001) are more suitable, although the computed frequency of the pressure drop fluctuations is somewhat too high. Because of the similarity between the results of these models and the large differences between the drag forces predicted by these models it is unlikely that the results can be improved by using yet another drag model. Because of its more fundamental basis the use of the Koch and Hill model is to be preferred.

## Notation

$a$ ratio between cube diameter and particle diameter, -
$C_D$ drag coefficient, -
$d$ diameter, m
$D$ distribution function, -
$e_n$ coefficient of normal restitution, -
$f$ volume fraction, -
$\mathbf{g}$ gravitational acceleration, m/s$^2$
$\mathbf{I}$ unit vector, -
$m_p$ particle mass, kg
$p$ pressure, Pa
$\mathbf{r}$ position, m
$\mathrm{Re}_p$ particle Reynolds number, -
$\mathbf{S}_p$ particle drag sink term, N/m$^3$
$t$ time, s
$\mathbf{u}$ gas velocity, m/s
$\mathbf{v}_p$ particle velocity, m/s
$V$ volume, m$^3$

**Greek Symbols**

$\beta$ inter-phase momentum transfer coefficient, kg/(m$^3$.s)
$\beta_0$ coefficient of tangential restitution, -
$\varepsilon$ volume fraction, -
$\lambda_f$ gas phase bulk viscosity, kg/(m.s)
$\mu_f$ gas phase shear viscosity, kg/(m.s)
$\mu$ dynamic friction coefficient, -
$\rho$ density, kg/m$^3$
$\boldsymbol{\tau}_f$ gas phase stress tensor, Pa
$\phi$ general variable
$\Phi$ flux, kg/(m$^2$.s)

**Subscripts**

*bg* background fluidization
*f* fluid phase
*mf* minimum fluidization
*p* particle
*sp* spout fluidization

$x$ horizontal direction
$w$ wall
$z$ vertical direction

## Acknowledgements

The authors would like to thank Hydro Agri Sluiskil, the Netherlands for their financial support to the project.

## References

Bird, R.B., Stewart, W.E. and Lightfoot, E.N., 1960. Transport phenomena, John Wiley & Sons, New York.

Ergun S., 1952. Fluid Flow through Packed Columns, Chemical Engineering Progress, 48, 89-94.

Goldschmidt, M.J.V., Kuipers, J.A.M. and van Swaaij, W.P.M., 2001. Hydrodynamic Modeling of Dense Gas-Fluidised Beds using the Kinetic Theory of Granular Flow: Effect of Coefficient of Restitution on Bed Dynamics, Chemical Engineering Science 56, 571-578.

Hoomans, B.P.B., Kuipers, J.A.M., Briels, W.J. and van Swaaij, W.P.M., 1996. Discrete Particle Simulation of Bubble and Slug Formation in a Two-Dimensional Gas-Fluidised Bed: A Hard-Sphere Approach, Chemical Engineering Science, 51-1, 99-118.

Kawaguchi, T., Sakamoto, M., Tanaka, T. and Tsuji, Y., 2000. Quasi-Three-Dimensional Numerical Simulation of Spouted Beds in Cylinder, Powder Technology, 109, 3-12.

Koch, D.L. and Hill, R.J., 2001. Inertial Effects in Suspension and Porous-Media Flows", Annual Reviews of Fluid Mechanics, 33, 619-647.

Link, J.M., Zeilstra, C., Deen, N.G. and Kuipers, J.A.M., 2004. Validation of a discrete particle model in a 2D spout-fluid bed using non-intrusive optical measuring techniques, Canadian Journal of Chemical Engineering, accepted for publication.

Littman, H., Morgan III, M.H., Narayanan, P.V., Kim, S.J. and Day, J.-Y., 1985. An Axisymmetric Model of Flow in the Annulus of a Spouted Bed of Coarse Particles. Model, Experimental Verification and Residence Time Distribution, Canadian Journal of Chemical Engineering, 63, 188-194.

Schiller, L. and Naumann, A., 1933. A drag coefficient correlation, VDI Zeitschrift, 77, 318-320.

Wen, Y.C. and Yu, Y.H., 1966. Mechanics of Fluidization, Chemical Engineering Progress Symposium Series, 62, 100-111.